



Density matrix renormalization group description of the island of inversion isotopes $^{28-33}\text{F}$ K. Fosseze ^{1,2,3} and J. Rotureau ⁴¹*FRIB Laboratory, Michigan State University, East Lansing, Michigan 48824, USA*²*Physics Division, Argonne National Laboratory, Lemont, Illinois 60439, USA*³*Florida State University, Tallahassee, Florida 32306, USA*⁴*Mathematical Physics, Lund University, S-221 00 Lund, Sweden*

(Received 11 May 2021; accepted 12 September 2022; published 19 September 2022)

Background: Recent experiments have confirmed that the neutron-rich isotopes $^{28,29}\text{F}$ belong to the so-called island of inversion (IOI), a region of the nuclear chart around $Z = 10$ and $N = 20$ where nuclear structure deviates from the standard shell model predictions due to deformation and continuum effects. However, while the general principles leading to the IOI are relatively well understood, the details of the low-lying structure of the exotic fluorine isotopes $^{28-33}\text{F}$ are basically unknown.

Purpose: In this work, we perform large-scale shell model calculations including continuum states to investigate the properties of the neutron-rich isotopes $^{25-33}\text{F}$, from a core of ^{24}O and using an effective two-body interaction with a small number of adjustable parameters in the central and tensor channels.

Methods: We develop two models adjusted on experimentally confirmed states in $^{25,26}\text{O}$ and $^{25-27}\text{F}$ based on different assumptions concerning the positions of the neutron $0d_{3/2}$ and $1p_{3/2}$ shells, and solve the many-body problem using the density matrix renormalization group (DMRG) method for open quantum systems in an sd - fp model space.

Results: We obtain the first detailed spectroscopy of $^{25-33}\text{F}$ in the continuum and show how the interplay between continuum effects and deformation explains the recent data on $^{28,29}\text{F}$. Several deformed one- and two-neutron halo states are predicted in $^{29,31}\text{F}$, and we provide some information about the possible structure of the heaviest fluorine isotopes. We also suggest several experimental studies of interest to constraint models and test the present predictions.

Conclusions: The complex structure of neutron-rich fluorine isotopes offers a trove of information about the formation of the southern shore of the IOI through a subtle interplay of emergent deformation via the neutron $p_{3/2}$ - $f_{7/2}$ coupling, and continuum effects favoring the occupation of the $1p_{3/2}$ shell over the $0d_{3/2}$ shell. Further experimental studies of this region will be essential to assess the quality of future theoretical approaches.

DOI: [10.1103/PhysRevC.106.034312](https://doi.org/10.1103/PhysRevC.106.034312)

I. INTRODUCTION

Exotic nuclei provide a unique window on the nature of the nuclear interaction and how nuclear systems self-organize [1,2], but also contribute to our understanding of long-standing problems such as the nucleosynthesis in the r process [3,4]. Compared to stable nuclei, their large N/Z asymmetry can produce dramatic rearrangements of nuclear structure with, for example, the emergence of deformation [5–8] and new “magic numbers” associated with new large shell gaps. Close to the drip lines, i.e. the limits of stability with respect to proton and neutron emission [9,10], exotic nuclei also reveal new stabilizing mechanisms such as the formation of halo structures [11].

These effects are exemplified in the so-called island of inversion (IOI), a neutron-rich region of the nuclear chart located between the neutron numbers $N = 20$ and $N = 28$ showing large quadrupole deformation and important continuum effects. The story behind the IOI can be roughly summarized as starting with the effect of tensor forces [12,13] and the mass dependence of the nuclear mean-field, which

slowly modify the positions of single-particle states as one moves away from the valley of β stability, effectively reducing the energy gap between the sd and fp shells. This shell evolution creates a situation where, in the shell model picture, the multipole part of the interaction [14] can lower the energy of the system by developing, for example, deformation through the residual quadrupole interaction coupling orbits satisfying $\Delta l = \Delta j = 2$ like the neutron shells $\nu 1p_{3/2}$ and $\nu 0f_{7/2}$, as beautifully explained in Elliott’s theory [15]. Nuclear deformation can also be seen as an instance of the Jahn-Teller effect [16], i.e., a spontaneous symmetry breaking due to the coupling of near-degenerate single-particle states [17–23]. For that reason, we will refer to the Elliott-Jahn-Teller effect since both theories describe the same phenomenon in two different pictures. In the present case of neutron-rich fluorine isotopes around $N = 20$, the near-degeneracy of the neutron shells $\nu 0d_{3/2}$ and $\nu 1p_{3/2}$ will also play a crucial role as we will show, but mostly due to their strong coupling to the continuum. Indeed, the final twist to the story is that, as deformation develops, the occupation of the $\nu 1p_{3/2}$ increases right when weak binding appears [24], creating an interplay between

continuum effects and deformation [22]. Of course, all these mechanisms derive from the nuclear interaction [25], which makes the IOI a particularly interesting place to test nuclear models. A complete review of the literature on the IOI can be found in Ref. [2].

The experimental study of this region is now feasible thanks to new technological developments on detectors and the construction of rare isotope beam facilities. More specifically, neutron-rich fluorine isotopes, located at the southern shore of the IOI with a proton number $Z = 9$, present a unique opportunity to challenge our understanding of nuclear forces. Indeed, just below the IOI, in oxygen isotopes ($Z = 8$), the neutron drip line extends up to $N = 16$ (^{24}O) and is well explained in a sd shell model space, while in fluorine isotopes it goes up to $N = 22$ (^{31}F) [26]. The story leading to the IOI gives an idea of how this sudden extension of the drip line happens, but so far no theoretical description including deformation and continuum couplings has been provided.

Series of measurements in ^{26}F [27–30] and ^{27}F [31–33] have clearly established that the low-lying spectra of these nuclei are dominated by sd shells, and, until recently, the same was believed about the ground state of ^{28}F [34] from the observation of a positive-parity ground state [35,36] compatible with standard shell model predictions. However, the situation changed after a new measurement giving a negative-parity ground state in ^{28}F [37], revealing that the $\nu 1p_{3/2}$ shell is already occupied in this isotope ($N = 19$). Compared to neutron-rich neon, sodium, or magnesium isotopes where the IOI starts at $N = 20$, this is an important change that needs to be understood.

Likewise, the first measurements of the isotope ^{29}F [32,33,38] gave a mass compatible with a $J^\pi = 5/2^+$ spin-parity assignment from the shell model, but the recent observation of a two-neutron halo in the ground state [39] suggests a stronger interplay between deformation and continuum effects than expected, potentially leading to a different spin-parity assignment. It will be interesting to see how the increasing role of the $\nu 1p_{3/2}$ shell noticed in $^{28,29}\text{F}$ affects the spectroscopy of the unbound ^{30}F and bound ^{31}F isotopes [40,41].

On the theory side, systematic calculations in the IOI essentially are of two types. There are density functional theory calculations of masses, radii, and quadrupole deformations in even-even nuclei [9,42], and large-scale shell model calculations. Concerning the latter, they can provide low-lying spectra, radii, and a trove of additional information about nuclear structure and the presence of deformation. For more information, see the excellent reviews in Refs. [43,44]. Notable studies on the IOI range from the pioneer works of Refs. [45,46] to modern applications of the shell model [47,48] and Monte Carlo shell model [25,49,50]. Hopefully, in the future *ab initio* methods will be able to provide much needed predictive power in the IOI [51]. There are, of course, many other valuable works on individual isotopes using various approaches, some of which will be mentioned in the Results section.

To our knowledge, except for the recent Gamow shell model calculations in ^{31}F [52] where significant truncations were applied, there is currently no large-scale study including

both continuum effects and the many-body correlations necessary to describe the emergence of deformation in neutron-rich fluorine isotopes. In this work, we make a modest attempt to include the necessary ingredients mentioned above with minimal truncations in a large model space and from ^{25}F up to ^{33}F . For that purpose, we apply the density matrix renormalization group (DMRG) method [53,54] to solve the shell model problem from a core of ^{24}O and including couplings to continuum states, and using minimal effective Hamiltonians designed to qualitatively capture known low-lying states in neutron-rich fluorine isotopes.

II. METHODS

The neutron-rich fluorine isotopes $^{25-33}\text{F}$ are described in the shell model picture starting from a core of ^{24}O , which has one-neutron and one-proton separation energies of $S_n = 4.19$ MeV and $S_p = 27.11$ MeV, respectively, and is associated with the new shell closure $N = 16$ [55]. The $^{24}\text{O}-n$ and $^{24}\text{O}-p$ interactions are modeled by two Woods-Saxon potentials as defined in Ref. [56], and whose parameters are adjusted on the single-particle states of ^{25}O and ^{25}F .

As mentioned in the previous section, the position of the neutron shell $\nu 1p_{3/2}$ plays a critical role in neutron-rich fluorine isotopes. We originally generated a first model “A” which reproduces reasonably well the low-lying spectra of light neutron-rich fluorine isotopes and gives a negative parity ground state in ^{28}F as seen experimentally, but at the cost of lowering the $\nu 0d_{3/2}$ shell to $E = -0.041$ MeV instead of $E = 0.776$ MeV ($\Gamma = 88$ keV) experimentally, and the $\nu 1p_{3/2}$ shell to $E = 0.298$ MeV ($\Gamma = 343$ keV) partly for numerical reasons as explained below. Unfortunately, we will see below that this model has a weak pairing interaction and hence leads to discrepancies with experiment when looking at the ground-state energy trend in heavier isotopes. Then, for comparison, we generated a second model “B” in which the $\nu 0d_{3/2}$ shell is at $E = 0.809$ MeV ($\Gamma = 87$ keV), close to its experimental value, and the $\nu 1p_{3/2}$ shell is at $E = 0.612$ MeV ($\Gamma = 1337$ keV) given by the same core potential. In addition, we imposed the ground-state energy trend to be closer to experiment while keeping in mind the increasing truncation effects with mass. The issue with this model is that, contrary to model A, it does not describe well light neutron-rich fluorine isotopes, but the agreement with experiment for $A > 27$ is much improved. Parameters for each model are given in Table II.

Because only four states in total could be used to constrain the nine parameters (including the charge radius R_{ch}), for both potentials, we first fixed the diffuseness d at 0.65 fm, since this value is fairly constant across the nuclear chart, and the potential radius R_0 using the standard formula $R_0 = r_0 A^{1/3}$ with $r_0 = 1.2$ fm. Then, we fixed the charge radius at $R_{\text{ch}} = 2.87$ fm as a compromise between experimental values in nuclei surrounding ^{24}O such as ^{18}O ($R_{\text{ch}} = 2.77$ fm) or ^{26}Ne ($R_{\text{ch}} = 2.92$ fm) and predictions from density functional theory [42] ($R_{\text{ch}} \approx 2.82$ fm) and *ab initio* methods [57] ($R_{\text{ch}} \approx 3.1$ fm) in ^{24}O . Only the depth V_0 and the spin-orbit term $V_{\ell s}$ were left free during the optimization. The parameters obtained as described above are shown in Table I

TABLE I. Parameters of the Woods-Saxon potentials representing the $^{24}\text{O}-n$ and $^{24}\text{O}-p$ interactions in both models. The columns denoted $\ell = 1$, $\ell = 2$, and $\ell = 3$ contain the readjusted parameters for the neutron p , d , and f waves, respectively. See text for details.

Parameter	Proton	Neutron	$\ell = 1$	$\ell = 2$	$\ell = 3$
Model A					
R_{ch} (fm)	2.87				
d (fm)	0.65	0.65	0.70		
R_0 (fm)	3.47	3.47	3.61		
V_0 (MeV)	68.74	47.50	49.50	49.50	
$V_{\ell s}$ (MeV fm 2)	3.795	10.8			
Model B					
d (fm)	0.65	0.65	0.70		
R_0 (fm)	3.47	3.47			
V_0 (MeV)	69.44	47.50	50.44	47.15	40.21
$V_{\ell s}$ (MeV fm 2)	4.183	10.8		10.55	10.33

(second and third columns) and are in reasonable agreement with those in Ref. [52].

In model A, the $\nu 0d_{3/2}$ and $\nu 1p_{3/2}$ shells were lowered compared to experiment not only to improve spectra in $^{26-27}\text{F}$, but also because the $\nu 1p_{3/2}$ shell would have had a width of about $\Gamma = 2.37$ MeV. In practice, a single-particle state with such a large width cannot be used directly in many-body calculations. Even though the order of the $\nu 0d_{3/2}$ and $\nu 1p_{3/2}$ shells has been changed, the energy gap between the two shells is still fairly small and the width of the $\nu 1p_{3/2}$ shell is still large enough to give this shell a more delocalized character than the $\nu 0d_{3/2}$ shell. In model B, the $\nu 0d_{3/2}$ shell was left at its experimental value and the large width of the $\nu 1p_{3/2}$ shell was dealt with numerically by using a basis in which both shells are weakly bound. We checked that the energy positions of the corresponding basis states did not affect the results due to the completeness of the single-particle basis. We note that the $\nu 0f_{7/2}$ shell is at $E = 2.90$ MeV in model A, while it is at $E = 5.23$ MeV in model B.

Another difference between the two models is that model B is defined in a smaller single-particle basis compared to model A. This was necessary to perform the optimization of the interaction in model B using information on the heaviest fluorine isotopes and with less truncations at the many-body level. Below, we describe the two model spaces used. The proton space comprises the $\pi d_{5/2}$ and $\pi s_{1/2}$ partial waves, each represented using the harmonic oscillator (HO) basis with $n_{\text{max}} = 10$ and 0 in models A and B, respectively, and with an oscillator length of $b = 2.0$ fm. This choice of basis is justified by the fact that the proton above ^{24}O in fluorine isotopes is always bound by more than 10 MeV and hence must have a well localized wave function.

On the other hand, the neutrons in neutron-rich fluorine isotopes are either weakly bound or unbound, and their wave function can be better expressed using the Berggren basis [58,59], which allows one to explicitly include resonant and scattering states at the single-particle level, and to naturally generalize the configuration interaction picture in the complex-energy plane [60].

This basis is built upon the selected eigenstates of a finite-range potential for each partial wave $c = (\ell, j)$ considered and is usually defined in the complex-momentum plane as

$$\sum_i |u_c(k_i)\rangle \langle \tilde{u}_c(k_i)| + \int_{\mathcal{L}_c^+} dk |u_c(k)\rangle \langle \tilde{u}_c(k)| = \hat{1}_c, \quad (1)$$

where the sum runs over the resonant states (or poles of the scattering matrix) selected, defined by their momenta k_i , and the integral goes over complex-energy scattering states along a contour \mathcal{L}_c^+ in the fourth quadrant which surrounds the poles included in the sum and then extends to $k \rightarrow \infty$.

The completeness of this basis is ensured by Cauchy's integral theorem, which means that the precise form of the contour \mathcal{L}_c^+ is unimportant, provided that all the selected poles lie between the contour and the real- k axis. For additional details see Ref. [60].

In the present work, the neutron space is comprised of the $\nu d_{3/2}$, $\nu p_{3/2}$, and $\nu f_{7/2}$ partial waves. We checked that adding additional partial waves did not affect the results significantly. Due to the large centrifugal barrier for $\ell = 3$ waves, which keeps the wave function localized, the $\nu f_{7/2}$ states are represented using the HO basis with $n_{\text{max}} = 5$ and 0 in models A and B, respectively, and with $b = 2.0$ fm.

Concerning the lower partial waves, in model A the $\nu d_{3/2}$ and $\nu p_{3/2}$ states are both represented in the Berggren basis by one decaying resonance ($0d_{3/2}$ and $1p_{3/2}$ shells, respectively) and discretized contours made of three segments defined by the following points in the complex momentum plane: $k_0 = 0.0$, $k_1 = (0.20, -0.05)$, $k_2 = 0.4$, and $k_3 = 4.0$ fm $^{-1}$ for $d_{3/2}$ shells, with each segment discretized by 8 scattering states using a Gauss-Legendre quadrature; and $k_0 = 0.0$, $k_1 = (0.25, -0.20)$, $k_2 = 0.5$, and $k_3 = 4.0$ fm $^{-1}$ for $p_{3/2}$ shells, with each segment discretized by 12 scattering states. In model B, we reduced the discretization to 5 and 7 scattering states per segment and changed the position of k_1 to $(0.20, -0.00)$ and $(0.20, -0.10)$ for the $\nu d_{3/2}$ and $\nu p_{3/2}$ partial waves, respectively.

We finally obtain a single-particle basis in model A (B) made of 22 (2) proton shells and 67 (39) neutron shells, from which Slater determinants (SDs) can be built as usual. Before discussing the nucleon-nucleon (NN) interaction in the valence space and its optimization, below, we introduce the many-body method used in this work.

One notes that a naive evaluation of the dimension of the Hamiltonian in ^{33}F gives $d = \binom{22}{N_p} \binom{67}{N_n} \approx 10^{11}$ in model A, which is already beyond the capabilities of most shell model codes. For that reason, the many-body problem is solved in the configuration-interaction picture using the density matrix renormalization group (DMRG) method for open quantum systems [53,54].

This powerful many-body method, originally introduced in condensed matter physics [61,62] and later imported in nuclear physics [63–68], can handle large model spaces by dividing the problem into two subspaces \mathcal{A} and \mathcal{B} corresponding to the “system” and the contributions from the medium or environment.

The space \mathcal{A} is fixed and composed of the many-body states $|i_A(j_A)\rangle$ built from a small number of selected

single-particle states, where i_A is the index of the state and j_A its total angular momentum, and it is assumed that the solution $|\Psi_0(J^\pi)\rangle$ in this subspace is a reasonably good approximation of the full solution $|\Psi(J^\pi)\rangle$. The DMRG strategy to solve the many-body problem efficiently consists of refining the starting approximation in the reference space, by gradually including relevant contributions from the medium while rejecting unnecessary contributions according to the DMRG truncation scheme.

At the first iteration, one single-particle state from the medium is added into the subspace \mathcal{B} (empty at first), and all the many-body states $|i_B(j_B)\rangle$ in \mathcal{B} are built and then coupled to those in \mathcal{A} to form the states $\{|i_A(j_A)\rangle \otimes |i_B(j_B)\rangle\}^{J^\pi}$ in which the shell model problem is solved giving a solution of the form

$$|\Psi(J^\pi)\rangle = \sum_{i_A, i_B} c_{i_A(j_A)}^{i_B(j_B)} [|i_A(j_A)\rangle \otimes |i_B(j_B)\rangle]^{J^\pi}. \quad (2)$$

In the present work, since the problem is not variational with the use of complex energies, the retained solution in $\mathcal{A} \otimes \mathcal{B}$ is the one that has the maximal overlap with the initial solution in the reference space $|\Psi_0(J^\pi)\rangle$. From this solution, the density matrix reduced in the reference space is calculated for each block j_B as

$$\rho(i_B, i'_B)(j_B) = \sum_{i_A} c_{i_A(j_A)}^{i_B(j_B)} c_{i_A(j_A)}^{i'_B(j_B)}, \quad (3)$$

and is then diagonalized to obtain the eigenvectors $\{|\alpha\rangle_B\}$ and eigenvalues $\{w_\alpha\}$. This is where the DMRG truncation operates and reduces dramatically the computational cost. The eigenvectors are ordered by decreasing $|w_\alpha|$ and one keeps in the subspace \mathcal{B} only the first N_ρ vectors so that the following condition is satisfied:

$$\left| 1 - \operatorname{Re} \left(i \sum_{\alpha=1}^{N_\rho} w_\alpha \right) \right| < \varepsilon, \quad (4)$$

where ε is the DMRG truncation. Of course, in the limit $\varepsilon \rightarrow 0$ results are exact. At the next iteration, a new single-particle state from the medium is added into \mathcal{B} , and the same procedure is repeated until the contributions of all the states in the medium have been absorbed.

This is called the warm-up phase and it is typically insufficient to reach convergence unless $\varepsilon \rightarrow 0$ as some many-body correlations have been lost at each iteration, and for that reason it should be followed by sweep phases [54]. However, the use of the Berggren basis gives an advantage over this problem. Indeed, a Berggren basis is usually made of a small number of fairly localized states (bound states and resonances) and a large number of scattering states, that can be treated as a reference space and an environment, respectively, with a weak entanglement between the two, in the original spirit of the DMRG method.

To improve the convergence further, natural orbitals [69] generated from truncated DMRG calculations can be used to more efficiently capture many-body correlations as was done in Refs. [70–75]. However, in this work, the emergence of deformation in the continuum makes this method less attractive. Indeed, in a spherical approach deformation is expressed by a

strong mixing of various partial waves and large contributions from multiparticle-multihole excitations above the lowest energy Slater determinant in the reference space. To make the matter worse, due to the Berggren basis, the Hamiltonian is complex symmetric and thus one must extract solutions in the full space that are invariant with respect to changes in the definition of the continuum, which is impractical in large-scale calculations. Instead, at each DMRG iteration one selects the physical state from the renormalization group-transformed Hamiltonian that has the maximal overlap with the reference state, providing that a reference state reasonably close to the full solution can be constructed. For these reasons, generating natural orbitals from a truncated DMRG calculation can sometimes lead to a redefinition of the reference state which does not converge to a physical state, and thus one must try to converge the calculations directly in the original basis.

Furthermore, even for a quasiexact direct calculation with a small value of ε the energy can start to drift after a given number of iterations because of the identification problem. In such a case, we found that simply reordering the single-particle shells based on their contribution to the energy during a truncated calculation, even when the energy drifted toward the end, greatly stabilized the subsequent calculation. This reordering method is not as sophisticated as the use of natural orbitals or the reordering techniques in Ref. [76] based on quantum information theory methods, but it allows for a quick optimization ensuring minimal destabilization of the identification. After reordering, the convergence of the energy with the number of iterations (shells) typically looks like a decreasing exponential.

Finally and as mentioned previously, the quality of the DMRG reference state is critical to ensure the proper identification of many-body resonances, which means that a large reference space usually provides a better starting point at an increased computational cost. However, in applications using the Berggren basis, it is necessary to consider a reference space build using poles of the single-particle scattering matrix to ensure that the target state will be a physical state. We chose to include only the shells $\nu 0d_{3/2}$, $\nu 1p_{3/2}$, $\pi 0d_{5/2}$, and $\pi 1s_{1/2}$. In light isotopes, enlarging the reference space using, for example, f waves did not affect the results, but in larger isotopes $A \geq 30$ tests have shown that some binding energy could be gained. For that reason, the present interaction has a dependence on the reference space.

Now that the one-body interaction as well as the single-particle space are defined, and the many-body approach is specified, we turn our attention to the NN valence space interaction and its optimization. We start from the Furutani-Horiuchi-Tamagaki (FHT) finite-range two-body interaction [77,78], which contains central, spin-orbit, and tensor terms expressed in all spin-isospin channels (S, T) as described in details in Ref. [56], and we reduce it using effective scale arguments as was done in Ref. [75] for neutron-rich helium isotopes.

According to halo effective field theory [79,80], the leading-order terms should be in the central 1S_0 and 3S_1 interaction channels, which correspond to the $(S, T) = (0, 1)$ and $(1, 0)$ central terms in the FHT interaction, denoted V_c^{01} and V_c^{10} , respectively. Note that these two parameters were the

only ones well constrained in a Bayesian analysis of a global fit of light nuclei above a ${}^4\text{He}$ core [56].

In model A, our first strategy was to fix the parameter V_c^{01} on the ground-state energy of ${}^{26}\text{O}$ (two neutrons above the core), and then to adjust the second parameter V_c^{10} , which only acts on the pn interaction ($T = 0$), on the ground state of ${}^{26}\text{F}$. However, while the value of V_c^{01} obtained gave satisfactory results in ${}^{26-28}\text{O}$, there was no value of V_c^{10} that could give the correct experimental ordering of the multiplet $J^\pi = 1^+, 2^+, 4^+, 3^+$ in ${}^{26}\text{F}$ (we obtained $4^+, 1^+, 2^+, 3^+$), even though we had the correct energy trend up to ${}^{31}\text{F}$.

This was an indication that the leading-order terms were not enough and small additional contributions must be considered. While in principle the tensor terms V_t^{10} and V_t^{11} should be important [12,13] because the dominant configuration of the multiplet is made of spin-orbit partner shells $j_{</>} = \ell \pm 1/2$, empirically, we found that they have a moderate effect in this case. Instead, only the central term V_c^{11} allows one to obtain the correct ordering of the spectrum in ${}^{26}\text{F}$, as well as the near degeneracy of the 2^+ and 4^+ states.

In fact, adding a small attractive tensor force overbinds the heaviest fluorine isotopes as more neutrons fill the $\nu 0d_{3/2}$ shell and they couple to the proton in the $\pi 0d_{5/2}$ shell. It is our understanding that, in ${}^{24}\text{O}$, the expected lowering of the $\nu 0d_{3/2}$ shell due to tensor forces has already been mostly absorbed by the one-body potential.

Finally, we adjusted the three selected parameters on the experimentally confirmed states in ${}^{26-28}\text{F}$ by solving the many-body problem exactly in ${}^{26-27}\text{F}$ and within a DMRG truncation denoted $4p4h-\varepsilon = 10^{-5}$ (see next section) in ${}^{28}\text{F}$, and obtained $V_c^{01} = -1.360$, $V_c^{10} = -1.244$, and $V_c^{11} = -68.00$ (all in MeV). This step was particularly difficult because of the lack of experimental data in general, and the fact that only the energy and parity of the ground state of ${}^{28}\text{F}$ are known. We generated many different sets of parameters fitting states in ${}^{26,27}\text{F}$ and postselected those giving a negative parity ground state in ${}^{28}\text{F}$ (any spin) and a reasonable energy position for the ground state of ${}^{29}\text{F}$ (any spin and parity). This required us to compute all the low-lying states in ${}^{28,29}\text{F}$ at every selection to ensure compliance with experimental data.

In contrast, we developed model B as an attempt to have a better energy trend in $A > 27$ isotopes compared to model A and thus used a different strategy. We assumed that the ground state of ${}^{31}\text{F}$ had a spin-parity of $J^\pi = 1/2^+$, which seemed reasonable since the $5/2^+$ state was already predicted close to the $1/2^+$ in model A and in a large-scale shell model [48], and found out that we needed to add a tensor force in the $(S, T) = (1, 1)$ channel to correct the energy trend and the discrepancy in the ground-state energy of ${}^{28}\text{F}$ seen in model A. However, the ordering of the states in ${}^{26}\text{F}$ was negatively affected and the the $5/2^+ - 1/2^+$ energy gap in ${}^{27}\text{F}$ was increased significantly. The optimization in ${}^{31}\text{F}$ was done within a $4p4h-\varepsilon = 10^{-5}$ DMRG truncation (see next section) to include as much many-body correlations as possible while ensuring the practical feasibility of the calculations. Unfortunately, the present truncation might not have been enough to fully capture deformation at this point, leading to a ground-state energy higher than experiment. The parameters

TABLE II. Experimental [30,81,82] and fitted energies with respect to the ${}^{24}\text{O}$ ground state (in MeV) and widths (in keV). (†) The experimental ground state of ${}^{28}\text{F}$ originally assigned to $J^\pi = 4^-$ in Ref. [37] was changed to 2^- in the fit (see text for details). (‡) In model B, the ground state of ${}^{28}\text{F}$ is the 1^- state at $E = -17.43$ MeV

Nucleus	J^π	E_{expt}	Model A	Model B
${}^{25}\text{O}$	$3/2^+$	0.776	-0.041	0.809
${}^{25}\text{F}$	$5/2^+$	-14.43	-14.29	-14.88
	$1/2^+$	-12.71	-12.94	-12.11
	$3/2^+$	-11.03	-10.94	-11.18
${}^{26}\text{F}$	1^+	-15.21	-15.83	-15.10
	2^+	-14.55	-15.14	-15.19
	4^+	-14.57	-14.87	-14.89
${}^{27}\text{F}$	$5/2^+$	-17.32	-17.46	-17.36
	$1/2^+$	-16.54	-16.34	-15.71
${}^{28}\text{F}$	2^- †	-17.10	-17.64	-17.37‡
${}^{31}\text{F}$	$1/2^+$	-18.67		-17.87

obtained for model B are $V_c^{01} = -1.884$, $V_c^{10} = -2.214$, and $V_c^{11} = -73.77$ (all in MeV), and $V_t^{11} = 26.17$ MeV fm $^{-2}$. We note that, because single-particle states are higher in energy in model B compared to model A, the two-body interaction is more attractive overall. In particular, the parameter V_c^{01} responsible for the $(J, T) = (0, 1)$ pairing interaction is about 38% more attractive than in model A.

Additionally, as in standard shell model calculations, we multiplied the interaction matrix elements by a mass-dependent factor $[(A_c + 2)/A]^{1/3}$ where A_c is the core mass and A the mass. The results are shown in Table II.

In Ref. [37], it was established experimentally that the ground state of ${}^{28}\text{F}$ has a negative parity, but its spin was assigned to $J^\pi = 4^-$ using spectroscopic factors from the standard shell model. However, in our calculations including continuum couplings, we obtained $J^\pi = 2^-$ as the ground state in all fits and decided to use this assignment in the optimization.

Compared to the Gamow shell model study of ${}^{31}\text{F}$ in Ref. [52], where the same interaction was optimized using seven parameters in a much smaller model space, we only needed three parameters in model A and four in model B. Our parameter V_c^{11} is comparatively similar to the one in Ref. [52], but V_c^{01} and V_c^{10} differ significantly. Note that, in our case, V_c^{01} and V_c^{10} are about the same size, which is consistent with their physical role as leading order terms from an effective scale perspective, and the result of a similar optimization of this interaction in light nuclei [56].

To summarize, the readjustment of the core parameters in model A, which was necessary to qualitatively describe known states in light fluorine isotopes, effectively led to a weakening of pairing correlations, which was corrected to some extent in model B at the price of a degradation of the results in light isotopes. In model A, the energy difference $S_n({}^{27}\text{F}) - S_n({}^{26}\text{F})$ is about 0.09 MeV instead of 1.33 MeV experimentally, while it is about 1.86 MeV in model B. Moreover, other important energy differences are improved in model B, such as $S_n({}^{26}\text{O}) = 0.794$ MeV (expt.) obtained at 1.05 MeV (A) and 0.833 MeV (B), $S_n({}^{26}\text{Ne}) = 18.17$ MeV

(expt.) obtained at 16.53 MeV (A) and 17.64 MeV (B), $\Delta_{2^+_{-0^+}}(^{26}\text{O}) = 1.316$ MeV (expt.) obtained at 1.05 MeV (A) and 1.237 MeV (B), and $\Delta_{2^+_{-0^+}}(^{26}\text{Ne}) = 2.02$ MeV (expt.) obtained at -0.36 MeV (A) and 1.33 MeV (B), where $\Delta_{2^+_{-0^+}}$ represents the energy difference between the first 2^+ and 0^+ states.

III. RESULTS

In this section, we first compare to experiment the ground-state energies of $^{25-33}\text{F}$ with respect to the ground state of ^{24}O obtained using both models, and then discuss the spectroscopy of each system and analyze the occupation numbers of different partial waves in the wave function to illustrate the emergence of deformation around $N = 20$ and its interplay with continuum couplings.

A. Energy trend in $^{25-33}\text{F}$ and position of the drip line

In all the calculations presented below, the many-body problem is solved exactly for $^{25-28}\text{F}$, while in $^{29-33}\text{F}$ the many-body basis is truncated by allowing only up to four particle-hole excitations (“4p4h”) above the lowest Slater determinant. In model A, the DMRG truncation is lowered to $\varepsilon = 10^{-8}$, which renders the results essentially independent of ε , while in model B we only considered $\varepsilon = 10^{-6}$ for practical reasons. Because of the larger model space considered in the final calculations, some differences appear with the results of the fit.

In Ref. [52], a different choice was made where a 2p2h truncation was applied above a small many-body space built using only the pole states at the single-particle level. Compared to such a truncated space, our near complete calculations gave energy differences of 0.5–3.0 MeV.

While the DMRG truncation set by ε allows one to obtain almost converged energies for all neutron-rich fluorine isotopes, the dependence of our results on the size of the reference space does not allow us to calculate widths precisely in all cases. It has been noted in Ref. [83] that widths are notoriously challenging to calculate in states with many active nucleons. For that reason, we can only provide reliable widths up to ^{28}F , and only indicate whether or not a state is narrow in heavier isotopes.

The ground-state energies of $^{25-33}\text{F}$ with respect to the ground state of ^{24}O obtained using both models are compared to experiment in Fig. 1. The overall energy trend is respected but, when looking at $A > 29$ isotopes, one can notice that both models underbind, most likely because deformation appears around $A = 29$ and the DMRG truncation, which gets worse as the mass increases, does not allow to fully capture deformation. In model A, the energy even decreases slightly with increasing A , which is a sign that the model might also require fine tuning in the $A > 29$ isotopes.

In lighter isotopes, while model A gets the ordering of energy spectra better than model B, as will be shown below, it significantly overbinds in ^{26}F and ^{28}F . In the latter case, the ground state of ^{28}F gained about 700 keV between the $\varepsilon = 10^{-5}$ truncation of the fit and the almost exact result, making it an outlier. We believe that the optimization of the

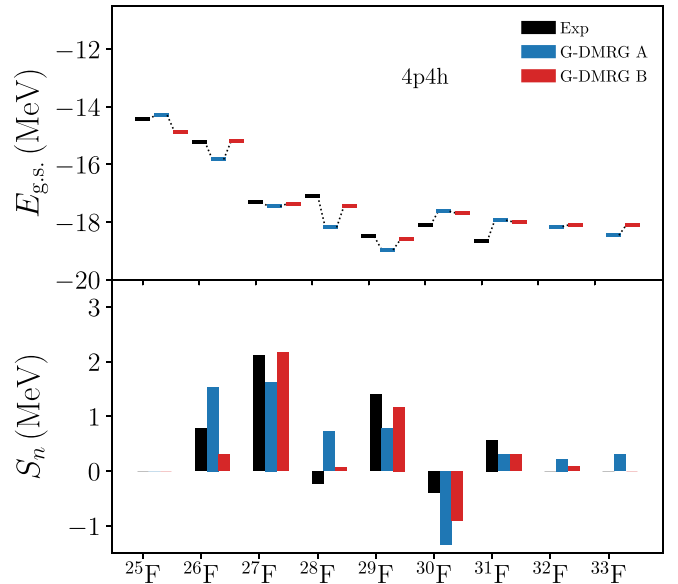


FIG. 1. Top panel: ground-state energies in $^{25-33}\text{F}$ with respect to the ^{24}O core. Experimental data [81] are compared to the results obtained exactly or almost in $^{25-28}\text{F}$ and with the DMRG truncation 4p4h in $^{29-33}\text{F}$ in both models. We note that in Ref. [81] the energies for $^{30,31}\text{F}$ are not measurements but estimates. Bottom panel: one-neutron separation energies in MeV.

two-body interaction in model A did not sufficiently capture pairing effects and overcompensated in this system by generating too much deformation.

In addition to the ground-state energies, the one-neutron separation energies S_n are shown in Fig. 1. While both models reproduce qualitatively the S_n values in most isotopes, significant discrepancies are found in ^{28}F where the sign of S_n is incorrect, notably for model A (see below), and also in ^{30}F because of underbinding, which we believe is due to many-body truncations.

Including the proton $d_{3/2}$ shells did not change the results at all, and, for instance, increasing the number of neutron $f_{7/2}$ shells or adding neutron $p_{1/2}$ shells in model A had an impact of less than 100 keV overall. Overall, even though we do not obtain all the threshold with a satisfactory precision, the choice of the Hamiltonian, model space, and the constraints applied give us models that take into account most of the experimental information available in the literature to some degree.

B. Detailed spectroscopy of $^{26-33}\text{F}$

In Figs. 2 and 3, we show the detailed spectroscopy of $^{26-29}\text{F}$ and $^{30-33}\text{F}$, respectively, where the ground-state energies are set to $E = 0$.

In ^{26}F , our results based on model A for positive parity states are in relative agreement with the most recent experimental results in Ref. [30] and the *ab initio* and phenomenological results mentioned therein, including the 3^+ which was not adjusted. However, we also predict negative parity states close to the 3^+ state, which were probably not produced in the one-proton knockout reactions used in

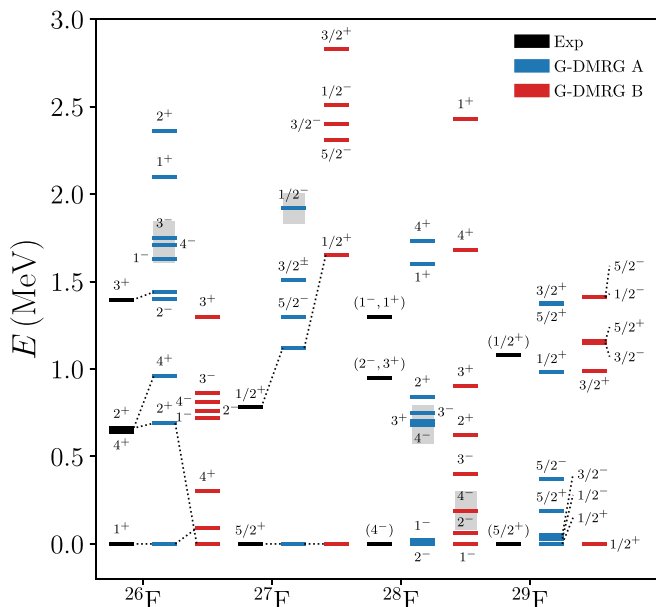


FIG. 2. Calculated energy levels in $^{26-29}\text{F}$ compared to experiment. The results for $^{26-28}\text{F}$ are virtually exact while those for ^{29}F are obtained with the 4p4h truncation. States with uncertain spin and parity assignments are written in parentheses.

Ref. [30] because of the initial state of the target. Finding experimentally the exact position of these negative parity states would be particularly valuable to constrain theoretical models by imposing strict conditions on the $\nu 1p_{3/2}$ single-particle state. As mentioned previously, model B does not reproduce well data in the lightest isotopes as it gives an incorrect ordering for the multiplet $J^\pi = 1^+, 2^+, 4^+, 3^+$. Also,

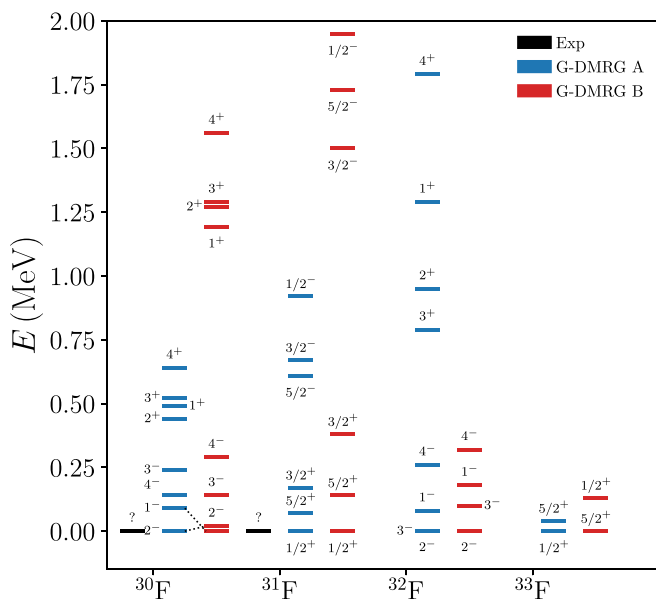


FIG. 3. Calculated energy levels in $^{30-33}\text{F}$ compared to experiment. Results are obtained with the 4p4h truncation. States with uncertain spin and parity assignments are written in parentheses.

all negative-parity states are found around the experimental 2^+ and 4^+ states.

In model A, the gap between the $5/2^+$ and $1/2^+$ states of ^{27}F that we obtained is too large but fairly robust, and is even larger in model B. One possible explanation is that some level of quadrupole deformation is already present in ^{27}F [84] but it cannot be fully accounted for in our model due to the spherical core of ^{24}O .

As in ^{26}F , in ^{27}F we also predict a mixing of positive and negative parity states above the first few low-lying states, whose experimental determination would be valuable for testing theoretical models.

The situation becomes more interesting in ^{28}F as there is a controversy about the spin of the ground state and about the exact nature of the excited spectrum. In model A, we predict a 2^- ground state essentially indistinguishable from a 1^- state, a group of positive and negative parity excited states about 700 keV higher where at least one state was observed with an uncertain spin and parity assignment [37], and two positive parity states slightly higher where again at least one state was observed. One notes that the *spdf-u-mix* shell model calculations [48] (refined in Ref. [37]) also predict clusters of states in these regions. The situation is similar in model B with a 1^- ground state almost degenerate with the 2^- state. The two remaining negative-parity states (3^- , 4^-) are predicted lower compared to model A, and the positive parity states are predicted at similar energy positions compared to model A, except for the 1^+ state which is predicted higher.

The situation in ^{29}F is rather intriguing. On the one hand, the standard shell model predicts a $5/2^+$ ground state with a small occupation of the $\nu p_{3/2}$ partial wave. In fact, as noted in Ref. [85], this was the result obtained in the Gamow shell model calculations of Ref. [52] limited to a 2p2h truncation. On the other hand, a recent experimental observation [39] showed that the ground state of ^{29}F presents a significantly enlarged radius compared to lighter fluorine isotopes, establishing the presence of a halo structure and suggesting a large weight of the $\nu p_{3/2}$ partial wave.

Interestingly, the shell model study based on the EEdf1 interaction [86] reported in Ref. [39] predicts a $5/2^+$ ground state, but also a possible excited state (presumably $1/2^+$) just above the ground state. While this study does not include continuum effects, it goes beyond the 2p2h truncation and hence better describes deformation.

In the present work, where we include continuum effects and go up to the 4p4h truncation, both models predict a $1/2^+$ ground state with a pair of neutrons in the $\nu p_{3/2}$ partial wave and another pair in the $\nu d_{3/2}$ partial wave. The finding of a $1/2^+$ ground state in ^{29}F would suggest the presence of a deformed two-neutron halo structure compatible with the recent observation. In model A, two negative parity states are predicted right above the $1/2^+$ state, as well as a $5/2^+$ state slightly higher, while in model B the $1/2^+$ state is isolated and the next excited state is about 1.0 MeV higher, where an excited state has been found experimentally.

Surprisingly, and contrary to all the low-lying states in ^{29}F , model A predicts the $5/2^+$ state to have a regular shell model structure with basically four neutrons in the $\nu d_{3/2}$ shells and

hence a negligible occupation of the $\nu p_{3/2}$ shells, and it could even be spherical as a consequence. This is rather surprising as, in principle, nothing prevents contributions of the form $(\pi d_{5/2})^1(\nu d_{3/2})^2(\nu p_{3/2})^2$ to the wave function, which would likely lead to deformation thanks to the Elliott-Jahn-Teller effect. If the prediction of model A for the $5/2^+$ state is correct, experimentally, the expected lack of a halo tail in its density profile could easily be misunderstood as the result of the pairing antihalo effect [87,88]. In contrast, model B predicts on average one neutron in the $\nu p_{3/2}$ shells and three in the $\nu d_{3/2}$ shells, suggesting a one-neutron halo. However, a closer look at the structure reveals that this state is dominated by a mix of the $(\pi d_{5/2})^1(\nu d_{3/2})^2(\nu p_{3/2})^2$ and $(\pi d_{5/2})^1(\nu d_{3/2})^4$ configurations.

Model A also predicts a $1/2^+$ excited state at about 1.0 MeV above the ground state where a bound $1/2^+$ state was found experimentally [33], and two positive parity excited state at about 1.4 MeV. All three states have significant occupations of the $\nu p_{3/2}$ partial wave. In comparison, model B predicts a $3/2^+$ state close to the $5/2^+$ state at about 1.0 MeV above the ground state, and the negative parity states at about 1.4 MeV, but we did not find excited $1/2^+$ and $5/2^+$ states. We attribute these differences between the two models to the role played by the $\nu 1p_{3/2}$ shell. This shell is relatively low in model A, which pushes negative parity states lower in energy compared to model B.

In conclusion, the experimental confirmation of a halo structure in ^{29}F reported in Ref. [39] is consistent with a $1/2^+$ ground state, but theoretical uncertainties in model A do not rule out a possible negative parity state ($1/2^-$ or $3/2^-$) with a large occupation of $\nu p_{3/2}$ shells. However, a $5/2^+$ ground state seems highly unlikely in both models.

The spectra of the heavier isotopes $^{30-33}\text{F}$ are shown in Fig. 3.

In ^{30}F , the progressive compression of the spectrum visible in $^{26-29}\text{F}$ reaches its maximum in model A with all the negative (positive) parity multiplet states located in the lower (upper) part of the spectrum and all below 1.0 MeV. This is simply a consequence of the increasing occupation of the $\nu 1p_{3/2}$ shell pushing negative parity states down. As in ^{28}F , we predict a $J^\pi = 2^-$ ground state but the spin is not firm due to theoretical uncertainties. In model B, the positive- and negative-parity multiplets stay well separated with all the former being around 1.2 MeV above the ground state, and the latter below 500 keV like in model A.

Being the last bound fluorine isotope, ^{31}F is particularly interesting. Using both models, we predict a $1/2^+$ ground state with two neutrons in the $\nu p_{3/2}$ partial wave as in ^{29}F , followed by two positive parity states close in energy ($5/2^+$, $3/2^+$) and negative parity states at higher energy.

Earlier shell model studies in the sd - fp space [48] predicted a $5/2^+$ ground state, but had already noticed a drastic reduction of the gap between the $5/2^+$ and $1/2^+$ states in ^{31}F due to deformation, with both states being dominated by intruder configuration by about 70%. Additional details on the inversion of the $5/2^+$ and $1/2^+$ states will be provided below.

In $^{32,33}\text{F}$, model A fails to provide the correct behavior for the ground-state energy trend as it decreases slightly with the mass number, most likely due to the lack of pairing interaction

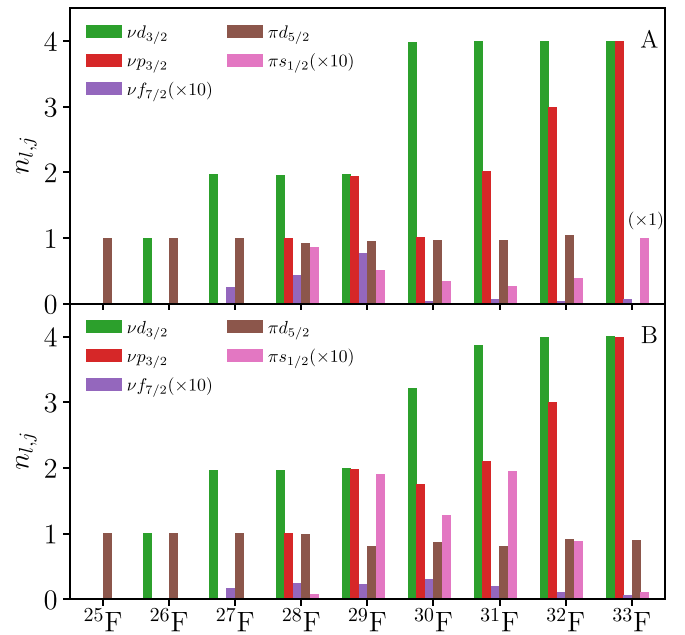


FIG. 4. Occupation numbers of the neutron and proton partial waves for the ground states in $^{25-33}\text{F}$ in models A (top panel) and B (bottom panel).

and the effect of many-body truncations. The issue with pairing is partially solved in model B, which gives an essentially flat ground-state energy trend instead. In ^{32}F , both models predict the positive-parity states to be pushed up in energy compared to the situation in ^{30}F , to the point that in model B they were too unstable to be converged in DMRG. In addition, both models predict the $5/2^+$ and $1/2^+$ states to be close in energy in ^{33}F , with the inversion of configuration persisting in model A.

Finally, to provide a more complete picture of the evolution of the structure of neutron-rich fluorine isotopes $^{25-33}\text{F}$, the occupations $n_{\ell,j}$ of different partial waves (ℓ, j) in the ground states are shown in Fig. 4.

Obviously, in a given system the sum of the occupations over all partial waves must give the number of particles in the valence space. Also, we need to be careful not to interpret the occupations of the partial waves as the occupations of the single-particle states in our basis or of individual configurations. An occupation of 2.0 in a given partial wave (ℓ, j) could mean, for example, that on average two particles occupy to some degree all the shells (n, ℓ, j), and thus could be mostly scattered in the continuum in our case.

The emergence of deformation already visible in the energy spectra in Figs. 2 and 3 becomes clearer when looking at the occupation numbers. As mentioned before, the first break from the standard shell model picture happens in ^{28}F where one would expect a positive parity ground state with about three neutrons in the $\nu d_{3/2}$ shells. Instead, as shown in Fig. 4, the negative-parity ground state of ^{28}F has occupations of about 2.0 and 1.0 in the $\nu d_{3/2}$ and $\nu p_{3/2}$ shells, respectively. Moreover, there is a substantial increase in the role of the $\nu f_{7/2}$ and $\pi s_{1/2}$ shells, which could indicate some deformation. We note that deformation is more present in model B, as revealed

by the significantly larger occupation of the $\pi s_{1/2}$ partial wave compared to model A. The interesting consequence of this result is that deformation might be induced by couplings to the continuum in ^{28}F since they enhance the occupation of the $\nu p_{3/2}$ partial wave leading to the Elliott-Jahn-Teller effect via the $p_{3/2}$ - $f_{7/2}$ quadrupole coupling. Note that the same can be said about the 1^- state at about the same energy.

A similar picture emerges as well in the ground state of ^{29}F , where the additional neutron goes into the $\nu p_{3/2}$ shells, giving the $\nu d_{3/2}$ and $\nu p_{3/2}$ shells almost equal weights in the wave function. This suggests a significant level of deformation in the ground state of ^{29}F , which translates into contributions beyond the 2p2h truncation having a large weight in the wave function.

Then, rather surprisingly, in model A the $\nu p_{3/2}$ partial wave in ^{30}F is partially depleted with an average occupation of about 1.0 compared to about 2.0 in ^{29}F , while the occupation of the $\nu d_{3/2}$ partial wave increases to about 4.0 and the $\nu f_{7/2}$ stops playing any significant role. One also notes a decrease in the weight of the $\pi s_{1/2}$ shells compared to $^{28,29}\text{F}$. Model B gives a different picture in which the $\nu p_{3/2}$ partial wave stays occupied by about two neutrons on average, and the occupation of the $\nu f_{7/2}$ shell stays significant, suggesting more deformation in this model. In $^{31-33}\text{F}$ the additional neutrons simply occupy the $\nu p_{3/2}$ shells in model A, and in ^{33}F the proton occupies the $\pi s_{1/2}$ shells instead of the $\pi d_{5/2}$ shells to couple to $J^\pi = 1/2^+$. A similar picture can be seen in model B, but with a higher occupation of the $\pi s_{1/2}$ shell and a $J^\pi = 5/2^+$ ground state in ^{33}F .

Experimentally, it would be interesting to test the validity of the picture presented here by looking at the neutron decay of ^{30}F . While asymptotic normalization coefficients could not be extracted readily in the present approach, it is not difficult to see that the occupations shown in Fig. 4 suggest a limited overlap between the ground state wave functions of ^{29}F and ^{30}F in model A, or for that matter any negative parity state in ^{30}F . In fact, as will be detailed in the next sections, the first $5/2^+$ state of ^{29}F should have a relatively larger overlap with the ground state of ^{30}F in model A.

C. Evolution of the $5/2^+$ and $1/2^+$ states

To investigate the evolution of the $5/2^+$ and $1/2^+$ states noted in $^{29,31,33}\text{F}$, in Fig. 5, we show the evolution of the occupations $n_{\ell,j}$ for the lowest $5/2^+$ and $1/2^+$ states in both model A (left panels) and model B (right panels). The energy differences $\Delta_{5/2^+-1/2^+} = E(5/2^+) - E(1/2^+)$ between these states are also shown and compared to experiment in the top panel to illustrate the evolution.

First, the evolution of the energy difference $\Delta_{5/2^+-1/2^+}$ in the top panel shows an inversion, or at least a convergence, of the $5/2^+$ and $1/2^+$ states starting in ^{29}F in both models. In $^{25,27}\text{F}$, where experimental data are available, both models give the correct sign for $\Delta_{5/2^+-1/2^+}$, and otherwise the models qualitatively agree with each other within theoretical uncertainties.

In ^{29}F , the magnitude of the energy difference differs significantly between models A and B, which we believe comes from their different amounts of deformation predicted in the

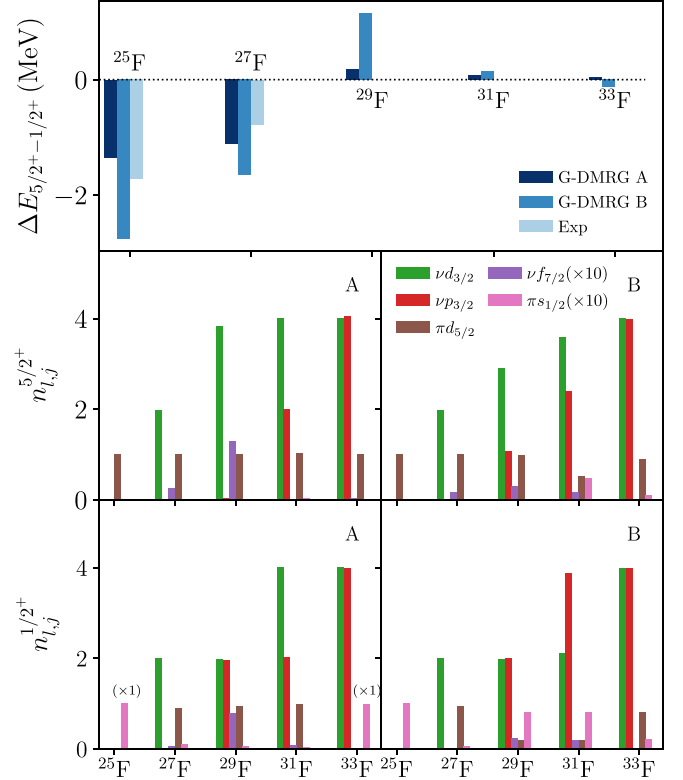


FIG. 5. Experimental and predicted energy differences between the lowest $J^\pi = 5/2^+$ and $1/2^+$ states in the $A = 25-33$ odd fluorine isotopes (upper panel), and corresponding occupation numbers of the neutron and proton partial waves for the $5/2^+$ (middle panels) and $1/2^+$ (lower panels) states in models A (left panels) and B (right panels). The occupation numbers for the $\nu f_{7/2}$ and $\pi s_{1/2}$ shells have been multiplied by 10.0 (unless indicated otherwise).

$5/2^+$ state. Indeed, both models predict similar occupations in the $1/2^+$ state of ^{29}F but, according to model A, in the $5/2^+$ states the single proton occupies almost exclusively the $\pi d_{5/2}$ partial wave, while the neutrons fill the $\nu d_{3/2}$ shells first, and then the $\nu p_{3/2}$ shells as the mass number increases. In model B, which seems to have more deformation, a different picture emerges as the $\nu p_{3/2}$ partial wave is occupied, contrary to the situation in model A. This is most likely the source of the large difference seen in $\Delta_{5/2^+-1/2^+}$ (^{29}F) between the two models. A difference in occupations persists in ^{31}F as well, where model A predicts a lower occupation of the $\nu p_{3/2}$ partial wave than model B, but both models have substantial occupations of the $\nu d_{3/2}$ and $\nu p_{3/2}$ waves, which leads to similar values of $\Delta_{5/2^+-1/2^+}$ (^{31}F).

A look at the occupations in each partial wave reveals that on average the $1/2^+$ states in $A > 27$ isotopes have larger occupations of the $\nu p_{3/2}$ shells and a more complex structure than the $5/2^+$ states, which suggests that they have more deformation. In particular, in ^{29}F ($N = 20$), the $1/2^+$ wave function loses its single-particle character. In both models, the four neutrons occupy the $\nu d_{3/2}$ and $\nu p_{3/2}$ partial waves almost evenly, with a non-negligible contribution from $\nu f_{7/2}$ shells, while the proton occupies the $\pi d_{5/2}$ and $\pi s_{1/2}$ partial waves. We interpret this strong mixing of various proton and

neutron partial waves as the emergence of deformation in our calculations, or in other words, of Nilsson orbitals. We note that occupation numbers between the $1/2^+$ and $5/2^+$ are significantly different, which indicates that they must have different intrinsic structures and are not part of the same rotational band. As a consequence, the energy difference between these states must be sensitive to single-particle energies.

The results of this study are strikingly similar to those of the early shell model calculations in Ref. [45], showing the onset of deformation at $N = 20$ for $Z = 9$ to 13 (^{29}F to ^{33}Al). In this work, it was noted that even though configuration inversion could be obtained in a sd - $f_{7/2}$ space, adding the $\nu 1p_{3/2}$ shell was the key to obtain deformation. Similar observations were also made in large-scale sd - f shell model calculations [47,48,50], showing that deformation might be the mechanism pushing the drip line to $A = 31$ in fluorine isotopes, with a disappearance of the $N = 20$ shell closure in ^{29}F . We note in passing that, in Ref. [50], a lowering of the $\nu 1p_{3/2}$ shell yielded improved results in $A > 28$ fluorine isotopes. In addition, in a recent study of the role of quadrupole deformation and continuum couplings in $^{28,29,31}\text{F}$ based on relativistic mean-field theory [89], it was shown that $\ell = 1$ waves contribute significantly to the wave function in those systems, but deformation only develops fully in $^{29,31}\text{F}$.

D. Halo structures

As mentioned previously, a halo was observed in the ground state of ^{29}F [39], which we predict to be a $1/2^+$ state with an occupation of about 2.0 in the $\nu p_{3/2}$ shells, suggesting a deformed two-neutron halo structure. Experimentally, if reality is closer to model A, it should be possible to distinguish the $1/2^+$ state from the next two negative parity excited states $1/2^-$ and $3/2^-$ because they have occupations of about 0.67 and 0.55 in the $\nu p_{3/2}$ shells, respectively, and hence should appear as deformed one-neutron halo systems. Moreover, in model A the next excited state $5/2^+$ has a negligible $\nu p_{3/2}$ occupation and should not present any halo property. If, however, model B provides a better representation of ^{29}F , there should be a gap of about 1.0 MeV between the ground state and the first excited state, and all excited states should present a halo structure if bound. In fact, one bound excited state was reported in ^{29}F [33], which we identified as the second $1/2^+$ state in model A, and could be either the $3/2^+$, $5/2^+$, or $3/2^-$ state in model B.

The presence of a halo structure in the ground state of ^{29}F was also investigated using a three-body approach in Ref. [90], later updated in Ref. [85] using the new experimental results in Ref. [37], where different scenarios based on the positions of the relevant single-particle states were proposed to cover the lack of firm data in this region. Overall, these studies suggest a moderate halo formation, which is amplified when lowering the gap between the $\nu 0d_{3/2}$ and $\nu 1p_{3/2}$ states. A subsequent study of the electric dipole response [91] found that the inversion of parity in ^{28}F led to strong dineutron correlations in the $\nu 1p_{3/2}$ shell indicative of a two-neutron halo.

The next candidate for halo structures is the ^{31}F isotope. The presence of a halo in the ground state was already

suspected in shell model calculations [50], but no definitive conclusion could be reached without continuum couplings.

From a different perspective, in a three-body model [92], a spherical core of ^{29}F was assumed, even though shell model calculations indicate possible deformation in this system, and, by essentially playing with the energy gap between the $\nu 1p_{3/2}$ and $\nu 0f_{7/2}$ shells, it was shown that for a relatively large gap ($\gtrsim 0.7$ MeV) halos could be obtained in both ^{29}F and ^{31}F , without any deformation, while a small gap would lead to a new form of antihalo effect. This finding is consistent with the fact that $\nu f_{7/2}$ shells play a minor role in our calculations and do not prevent the formation of halo structures.

In Ref. [52], it was found from Gamow shell model [60] calculations that the tail of the radial density in the ground state of ^{31}F decreases polynomially and is associated with a substantial increase in the matter radius, as expected in halo nuclei. While this approach could in principle capture deformation, by applying a $2p2h$ truncation on the many-body basis, the correlations required to describe deformation were severely limited. For that reason, in Ref. [52] the halo obtained in the ground state of ^{31}F , be it $5/2^+$ or $1/2^+$, must come mostly from the occupation of the $\nu 1p_{3/2}$ shell in a strict single-particle sense, and less from the emergence of deformed (Nilsson) orbitals. Nevertheless, the presence of a halo structure in ^{31}F seems to be a robust feature.

In this work, the predicted $1/2^+$ ground state of ^{31}F has an occupation of the $\nu p_{3/2}$ partial wave of about 2.0 in both models, which is compatible with the presence of a deformed two-neutron halo. Interestingly, assuming the predicted spectrum in model A would not change with the correct thresholds, the next two excited states $5/2^+$ and $3/2^+$ could be bound since they are below the one-neutron emission threshold at about 570 keV. Both states have significant occupations in the $\nu p_{3/2}$ partial wave of about 2.0 and 2.1, respectively, and hence would likely present deformed halo structures.

IV. CONCLUSION

In this work, we performed large-scale shell model calculations of the low-lying states in $^{25-33}\text{F}$ using the DMRG method and including couplings to the continuum. We started from a core of ^{24}O and optimized two effective two-body interactions with a few adjustable parameters in a sd - f model space, and considered minimal truncations to properly describe the emergence of deformation together with continuum effects. The two models obtained differ mostly in the assumption made on the positions of the $\nu 0d_{3/2}$ and $\nu 1p_{3/2}$ shells during the optimization, which in turn led to differences in the strength of the pairing interaction and the amount of deformation. While these models are simple, they explain the most recent data on $^{28,29}\text{F}$ from two different pictures and provide predictions to be tested experimentally.

The main findings of this study are

- (i) The observed negative-parity ground state in ^{28}F can be explained as the result of continuum couplings inducing some deformation based on energy spectra and occupations of different partial waves.
- (ii) Negative-parity ground states are predicted in $^{30,32}\text{F}$.

- (iii) The halo structure observed in the ground state of ^{29}F is likely a deformed two-neutron halo $1/2^+$ state, and several one-neutron halo structures are predicted in the excited spectrum, with the exception of the first $5/2^+$ state (model A only) which should not present any halo.
- (iv) The ground state of ^{31}F is predicted to be a $1/2^+$ state and the three lowest states (including the ground state) are expected to present deformed two-neutron halo structures if bound.

Additionally, predictions are provided for excited states in $^{28-33}\text{F}$ and recommendations are made for experimental studies that could help to constraint models and improve our understanding of how the IOI emerges.

Beyond the large-scale nature of the calculations, the main difficulty encountered in this work was to determine a minimal Hamiltonian capable of describing the phenomenology of all neutron-rich fluorine isotopes, and in particular to properly account for the role of the $\nu p_{3/2}$ partial wave. For instance, our model B, which captures pairing and deformation better than model A and hence performs better in the heaviest isotopes, does not reproduce the parabolic behavior [93] expected in

the ^{26}F multiplet, suggesting that further improvements are possible. The development of *ab initio* approaches in this region could provide much needed predictive power for more precise methods.

In the context of the IOI, the present results are in line with previous studies in $Z = 10-13$ nuclei, except that in fluorine isotopes continuum effects already appear at $N = 19$ (^{28}F). We plan on studying neutron-rich $Z = 10-13$ nuclei including couplings to the continuum to understand the mechanisms leading to the further extension of the drip line in these nuclei.

ACKNOWLEDGMENTS

Useful discussions with Xingze Mao are gratefully acknowledged. We thank Alfredo Poves for an enlightening discussion on the link between Elliott's theory and the Jahn-Teller effect. This material is based upon work supported by the U.S. Department of Energy, Office of Science, Office of Nuclear Physics, under the FRIB Theory Alliance Award No. DE-SC0013617. An award of computer time was provided by the Institute for Cyber-Enabled Research at Michigan State University.

-
- [1] O. Sorlin and M. G. Porquet, *Prog. Part. Nucl. Phys.* **61**, 602 (2008).
 - [2] T. Otsuka, A. Gade, O. Sorlin, T. Suzuki, and Y. Utsuno, *Rev. Mod. Phys.* **92**, 015002 (2020).
 - [3] D. Martin, A. Arcones, W. Nazarewicz, and E. Olsen, *Phys. Rev. Lett.* **116**, 121101 (2016).
 - [4] M. R. Mumpower, R. Surman, G. C. McLaughlin, and A. Aprahamian, *Prog. Part. Nucl. Phys.* **86**, 86 (2016).
 - [5] P. Federman and S. Pittel, *Phys. Rev. C* **20**, 820 (1979).
 - [6] J. Dobaczewski, W. Nazarewicz, J. Skalski, and T. Werner, *Phys. Rev. Lett.* **60**, 2254 (1988).
 - [7] S. Pittel and P. Federman, *Int. J. Mod. Phys. E* **02**, 3 (1993).
 - [8] W. Nazarewicz, *Nucl. Phys. A* **574**, 27 (1994).
 - [9] J. Erler, N. Birge, M. Kortelainen, W. Nazarewicz, E. Olsen, A. M. Perhac, and M. Stoitsov, *Nature (London)* **486**, 509 (2012).
 - [10] L. Neufcourt, Y. Cao, S. A. Giuliani, W. Nazarewicz, E. Olsen, and O. B. Tarasov, *Phys. Rev. C* **101**, 044307 (2020).
 - [11] I. Tanihata, H. Savajols, and R. Kanungo, *Prog. Part. Nucl. Phys.* **68**, 215 (2013).
 - [12] T. Otsuka, R. Fujimoto, Y. Utsuno, B. A. Brown, M. Honma, and T. Mizusaki, *Phys. Rev. Lett.* **87**, 082502 (2001).
 - [13] T. Otsuka, T. Suzuki, R. Fujimoto, H. Grawe, and Y. Akaishi, *Phys. Rev. Lett.* **95**, 232502 (2005).
 - [14] M. Dufour and A. P. Zuker, *Phys. Rev. C* **54**, 1641 (1996).
 - [15] J. P. Elliott and P. G. Dawber, *Symmetry in Physics. Vol. 2: Further Applications*, 1st ed. (Oxford University Press, Oxford, 1979).
 - [16] H. A. Jahn and E. Teller, *Proc. R. Soc. A* **161**, 220 (1937).
 - [17] P. G. Reinhard and E. W. Otten, *Nucl. Phys. A* **420**, 173 (1984).
 - [18] W. Nazarewicz, *Prog. Part. Nucl. Phys.* **28**, 307 (1992).
 - [19] W. Nazarewicz, *Int. J. Mod. Phys. E* **02**, 51 (1993).
 - [20] H. Häkkinen, J. Kolehmainen, M. Koskinen, P. O. Lipas, and M. Manninen, *Phys. Rev. Lett.* **78**, 1034 (1997).
 - [21] W. Satuła, J. Dobaczewski, and W. Nazarewicz, *Phys. Rev. Lett.* **81**, 3599 (1998).
 - [22] I. Hamamoto, *Phys. Rev. C* **76**, 054319 (2007).
 - [23] I. Hamamoto, *Phys. Rev. C* **85**, 064329 (2012).
 - [24] I. Hamamoto and B. R. Mottelson, *Phys. Rev. C* **69**, 064302 (2004).
 - [25] N. Tsunoda, T. Otsuka, K. Takayanagi, N. Shimizu, T. Suzuki, Y. Utsuno, S. Yoshida, and H. Ueno, *Nature (London)* **587**, 66 (2020).
 - [26] D. S. Ahn *et al.*, *Phys. Rev. Lett.* **123**, 212501 (2019).
 - [27] N. Frank *et al.*, *Phys. Rev. C* **84**, 037302 (2011).
 - [28] M. Stanoiu *et al.*, *Phys. Rev. C* **85**, 017303 (2012).
 - [29] A. Lepailleur *et al.*, *Phys. Rev. Lett.* **110**, 082502 (2013).
 - [30] M. Vandebrouck *et al.*, *Phys. Rev. C* **96**, 054305 (2017).
 - [31] Z. Elekes *et al.*, *Phys. Lett. B* **599**, 17 (2004).
 - [32] L. Gaudefroy *et al.*, *Phys. Rev. Lett.* **109**, 202503 (2012).
 - [33] P. Doornenbal *et al.*, *Phys. Rev. C* **95**, 041301(R) (2017).
 - [34] A. Schiller, T. Baumann, J. Dietrich, S. Kaiser, W. Peters, and M. Thoennessen, *Phys. Rev. C* **72**, 037601 (2005).
 - [35] G. Christian *et al.*, *Phys. Rev. Lett.* **108**, 032501 (2012).
 - [36] G. Christian *et al.*, *Phys. Rev. C* **85**, 034327 (2012).
 - [37] A. Revel *et al.*, *Phys. Rev. Lett.* **124**, 152502 (2020).
 - [38] D. Guillemaud-Mueller *et al.*, *Z. Phys. A* **332**, 189 (1989).
 - [39] S. Bagchi *et al.*, *Phys. Rev. Lett.* **124**, 222504 (2020).
 - [40] H. Sakurai *et al.*, *Phys. Rev. C* **54**, R2802(R) (1996).
 - [41] H. Sakurai *et al.*, *Phys. Lett. B* **448**, 180 (1999).
 - [42] <http://massexplorer.frib.msu.edu>.
 - [43] T. Otsuka, M. Honma, T. Mizusaki, N. Shimizu, and Y. Utsuno, *Prog. Part. Nucl. Phys.* **47**, 319 (2001).
 - [44] E. Caurier, G. Martinez-Pinedo, F. Nowacki, A. Poves, and A. P. Zuker, *Rev. Mod. Phys.* **77**, 427 (2005).
 - [45] A. Poves and J. Retamosa, *Phys. Lett. B* **184**, 311 (1987).
 - [46] E. K. Warburton, J. A. Becker, and B. A. Brown, *Phys. Rev. C* **41**, 1147 (1990).

- [47] E. Caurier, F. Nowacki, A. Poves, and J. Retamosa, *Phys. Rev. C* **58**, 2033 (1998).
- [48] E. Caurier, F. Nowacki, and A. Poves, *Phys. Rev. C* **90**, 014302 (2014).
- [49] Y. Utsuno, T. Otsuka, T. Mizusaki, and M. Honma, *Phys. Rev. C* **60**, 054315 (1999).
- [50] Y. Utsuno, T. Otsuka, T. Mizusaki, and M. Honma, *Phys. Rev. C* **64**, 011301(R) (2001).
- [51] T. Miyagi, S. R. Stroberg, J. D. Holt, and N. Shimizu, *Phys. Rev. C* **102**, 034320 (2020).
- [52] N. Michel, J. G. Li, F. R. Xu, and W. Zuo, *Phys. Rev. C* **101**, 031301(R) (2020).
- [53] J. Rotureau, N. Michel, W. Nazarewicz, M. Płoszajczak, and J. Dukelsky, *Phys. Rev. Lett.* **97**, 110603 (2006).
- [54] J. Rotureau, N. Michel, W. Nazarewicz, M. Płoszajczak, and J. Dukelsky, *Phys. Rev. C* **79**, 014304 (2009).
- [55] K. Tshoo *et al.*, *Phys. Rev. Lett.* **109**, 022501 (2012).
- [56] Y. Jaganathen, R. M. Id Betan, N. Michel, W. Nazarewicz, and M. Płoszajczak, *Phys. Rev. C* **96**, 054316 (2017).
- [57] V. Lapoux, V. Somà, C. Barbieri, H. Hergert, J. D. Holt, and S. R. Stroberg, *Phys. Rev. Lett.* **117**, 052501 (2016).
- [58] T. Berggren, *Nucl. Phys. A* **109**, 265 (1968).
- [59] T. Berggren and P. Lind, *Phys. Rev. C* **47**, 768 (1993).
- [60] N. Michel, W. Nazarewicz, M. Płoszajczak, and T. Vertse, *J. Phys. G: Nucl. Part. Phys.* **36**, 013101 (2009).
- [61] S. R. White, *Phys. Rev. Lett.* **69**, 2863 (1992).
- [62] S. R. White, *Phys. Rev. B* **48**, 10345 (1993).
- [63] J. Dukelsky and G. G. Dussel, *Phys. Rev. C* **59**, R3005(R) (1999).
- [64] J. Dukelsky and S. Pittel, *Phys. Rev. C* **63**, 061303(R) (2001).
- [65] S. Pittel and J. Dukelsky, *Rev. Mex. Fis.* **47**, Suppl. 2, 42 (2001).
- [66] J. Dukelsky, S. Pittel, S. S. Dimitrova, and M. V. Stoitsov, *Phys. Rev. C* **65**, 054319 (2002).
- [67] S. Pittel and J. Dukelsky, *Rev. Mex. Fis.* **49**, Suppl. 4, 82 (2003).
- [68] T. Papenbrock and D. J. Dean, *J. Phys. G: Nucl. Part. Phys.* **31**, S1377 (2005).
- [69] L. Brillouin, *Acta Sci. India* **71**, 159 (1933).
- [70] Ik Jae Shin, Y. Kim, P. Maris, J. P. Vary, C. Forssén, J. Rotureau, and N. Michel, *J. Phys. G: Nucl. Part. Phys.* **44**, 075103 (2017).
- [71] K. Fosseze, J. Rotureau, N. Michel, Q. Liu, and W. Nazarewicz, *Phys. Rev. C* **94**, 054302 (2016).
- [72] K. Fosseze, J. Rotureau, N. Michel, and M. Płoszajczak, *Phys. Rev. Lett.* **119**, 032501 (2017).
- [73] K. Fosseze, J. Rotureau, N. Michel, and W. Nazarewicz, *Phys. Rev. C* **96**, 024308 (2017).
- [74] M. D. Jones, K. Fosseze, T. Baumann, P. A. DeYoung, J. E. Finck, N. Frank, A. N. Kuchera, N. Michel, W. Nazarewicz, J. Rotureau, J. K. Smith, S. L. Stephenson, K. Stiefel, M. Thoennessen, and R. G. T. Zegers, *Phys. Rev. C* **96**, 054322 (2017).
- [75] K. Fosseze, J. Rotureau, and W. Nazarewicz, *Phys. Rev. C* **98**, 061302(R) (2018).
- [76] O. Legeza, L. Veis, A. Poves, and J. Dukelsky, *Phys. Rev. C* **92**, 051303(R) (2015).
- [77] H. Furutani, H. Horiuchi, and R. Tamagaki, *Prog. Theor. Phys.* **60**, 307 (1978).
- [78] H. Furutani, H. Horiuchi, and R. Tamagaki, *Prog. Theor. Phys.* **62**, 981 (1979).
- [79] C. A. Bertulani, H. W. Hammer, and U. van Kolck, *Nucl. Phys. A* **712**, 37 (2002).
- [80] P. F. Bedaque, H. W. Hammer, and U. van Kolck, *Phys. Lett. B* **569**, 159 (2003).
- [81] <http://www.nndc.bnl.gov/ensdf> (2015).
- [82] Z. Vajta *et al.*, *Phys. Rev. C* **89**, 054323 (2014).
- [83] X. Mao, J. Rotureau, W. Nazarewicz, N. Michel, R. M. Id Betan, and Y. Jaganathen, *Phys. Rev. C* **102**, 024309 (2020).
- [84] A. O. Macchiavelli, R. M. Clark, H. L. Crawford, P. Fallon, I. Y. Lee, C. Morse, C. M. Campbell, M. Cromaz, and C. Santamaria, *Phys. Rev. C* **102**, 041301(R) (2020).
- [85] L. Fortunato, J. Casal, W. Horiuchi, J. Singh, and A. Vitturi, *Commun. Phys.* **3**, 132 (2020).
- [86] N. Tsunoda, T. Otsuka, N. Shimizu, M. Hjorth-Jensen, K. Takayanagi, and T. Suzuki, *Phys. Rev. C* **95**, 021304(R) (2017).
- [87] K. Bennaceur, J. Dobaczewski, and M. Płoszajczak, *Phys. Lett. B* **496**, 154 (2000).
- [88] K. Hagino and H. Sagawa, *Phys. Rev. C* **95**, 024304 (2017).
- [89] Y.-X. Luo, K. Fosseze, Q. Liu, and J.-You Guo, *Phys. Rev. C* **104**, 014307 (2021).
- [90] J. Singh, J. Casal, W. Horiuchi, L. Fortunato, and A. Vitturi, *Phys. Rev. C* **101**, 024310 (2020).
- [91] J. Casal, J. Singh, L. Fortunato, W. Horiuchi, and A. Vitturi, *Phys. Rev. C* **102**, 064627 (2020).
- [92] H. Masui, W. Horiuchi, and M. Kimura, *Phys. Rev. C* **101**, 041303(R) (2020).
- [93] K. L. G. Heyde, *The Nuclear Shell Model*, 1st ed. (Springer-Verlag, Berlin, 1990).